Composites Science and Technology 70 (2010) 546–550

Contents lists available at ScienceDirect

Composites Science and Technology

journal homepage: www.elsevier.com/locate/compscitech

Short communication

Investigation of carbon nanotube reinforced aluminum matrix composite materials

Hansang Kwon [a,*], Dae Hoon Park [a], Jean François Silvain [a], Akira Kawasaki [b,*]

[a] Institut de Chimie de la Matière Condensée de Bordeaux (ICMCB) du CNRS, 87 Avenue du Dr. Albert Schweitzer, Pessac 33608, France
[b] Department of Materials Processing Engineering, Graduate School of Engineering, Tohoku University, Sendai 980-8579, Japan

ARTICLE INFO

Article history:
Received 20 May 2009
Received in revised form 4 November 2009
Accepted 27 November 2009
Available online 4 December 2009

Keywords:
Carbon nanotubes
A. Metal–matrix composites (MMCs)
B. Mechanical properties
E. Powder processing

ABSTRACT

We have increased the tensile strength without compromising the elongation of aluminum (Al)–carbon nanotube (CNT) composite by a combination of spark plasma sintering followed by hot-extrusion processes. From the microstructural viewpoint, the average thickness of the boundary layer with relatively low CNT incorporation has been observed by optical, field-emission scanning electron, and high-resolution transmission electron microscopies. Significantly, the Al–CNT composite showed no decrease in elongation despite highly enhanced tensile strength compared to that of pure Al. We believe that the presence of CNTs in the boundary layer affects the mechanical properties, which leads to well-aligned CNTs in the extrusion direction as well as effective stress transfer between the Al matrix and the CNTs due to the generation of aluminum carbide.

1. Introduction

The fabrication of metal composites reinforced by CNTs [1–3] is currently falling behind as compared with polymer- and ceramic–CNT composites due to issues such as dispersion, bulk production of highly oriented CNTs, and interface strength [4–11]. These three difficult issues have to be addressed to obtain the next generation of metal–CNT composites. Previously, several approaches have been evaluated based on different methods, such as high-energy ball milling, cold isostatic pressing, hot extrusion, and a powder rolling technique, which resulted in small reinforcements in tensile strength for metal–CNT composites [12–17]. However, a metal–CNT composite that combines highly enhanced tensile strength and elongation properties has not hitherto been realized.

Spark plasma sintering (SPS) is a useful technique for the densification of unsinterable materials and for forming strong interfaces by utilizing its characteristic sintering principle [18–20]. The hot-extrusion method is commonly used for the direct fabrication of engineering materials with fine microstructure [21]. In our previous investigation, we achieved good dispersal of CNTs in Al powder and highly densified bulk production without problems of damage of the CNTs [18,22].

In the present work, we have investigated the interfacial characteristics of a boundary layer with relatively low CNT incorporation (1 vol.%) from the microstructural viewpoint. Moreover, we discuss the relationship between mechanical properties such as tensile strength or elongation and the boundary layer.

2. Experimental procedure

The average diameter and length of the raw multi-walled CNTs used (Iljin Co. Ltd., purity 99.5%) were 20 nm and 30 μm, respectively. The CNTs were firstly mixed with natural rubber (NR) in benzene as solvent by the NSD method [18,22–24]. Commercial gas-atomized pure Al powder (ECKA Granules Japan Co. Ltd., purity 99.85%, average particle size 14.82 μm) was then added. The volume ratio of CNTs to Al powder in the precursor was fixed at 1:99. More details of this process can be found in our previous reports [18,22,24]. The precursor mixture was heat-treated at 500 °C for 2 h in an argon atmosphere (1 L/min flow rate) in order to remove the NR employed. The obtained Al/CNT mixture (powder) was sintered in a carbon mold under a pressure of 50 MPa using a spark plasma sintering device (SPS-S515) made by Sumitomo Coal Mining Co. Ltd. The dimensions of the spark plasma sintered (SPSed) compact were 15 mm in diameter and 30 mm in length. The sintering temperature was varied according to the sequence 480, 500, 560, and 600 °C, and the heating rate and holding time were fixed at 40 °C/min and 20 min, respectively. SPSed compacts were extruded in a 60° conical die at 400 °C with a 500 kN press (UH-500 kN, Shimadzu Corporation). The extrusion velocity and extrusion ratio were fixed at 2 mm/min and 20, respectively.

The morphologies of the samples (Al–CNT powder, Al–CNT SPSed compact, and Al–CNT composite) subjected to the respective processes were observed by means of an optical microscope (PMG-3, Olympus, Japan), a field-emission scanning electron microscope

* Corresponding authors. Tel.: +33 5 4000 6248; fax: +33 5 4000 2167.
E-mail addresses: hansang@icmcb-bordeaux.cnrs.fr (H. Kwon), kawasaki@material.tohoku.ac.jp (A. Kawasaki).

0266-3538/$ - see front matter © 2009 Elsevier Ltd. All rights reserved.
doi:10.1016/j.compscitech.2009.11.025

(FE-SEM6500, JEOL Co. Ltd., Japan), and a high-resolution transmission electron microscope (HR-TEM, Hitachi HF-2000, Japan) using selected-area diffraction patterns (SADP). Raman spectroscopic measurements (SOLAR TII Nanofinder, Tokyo Instruments Co. Ltd., Japan) enabled determination of the I_D/I_G ratio depending on the CNTs after each process. For evaluation of tensile strength, the composites were machined into test pieces of diameter 3 mm in accordance with ICS 59.100.01. Tensile tests on three test pieces at each sintering temperature were carried out with a universal testing machine (AUTOGRAPH AG-I 50 kN, Shimadzu Co. Ltd., Japan).

3. Results and discussion

As can be seen in Fig. 1, in spite of debinding of the natural rubber during treatment at 500 °C for 2 h, no change was observed in the average particle size and spherical shape of Al compared to those of raw Al. The diameter of the CNTs was not changed, but they became shorter after the debinding process. However, it is believed that the debinding process employed does not significantly affect the morphology of the Al or the diameter of the CNTs, and the natural rubber was clearly decomposed from the Al–CNT mixture, at least from the microstructural viewpoint. Furthermore, the CNTs were uniformly and omnidirectionally dispersed onto the surfaces of each Al particle, as shown in Fig. 1b.

The spark plasma sintered (SPSed) compacts were successfully densified up to 96.8% relative density, as indicated in Table 1. In general, Al powder has low sinterability because the stable oxide layer on the surfaces of the Al particles prevents their direct contact [18–20]. We attribute the achievement of high density to a certain degree of destruction of the oxide layers by the spark plasma and the applied pressure during the SPS process [18–20].

Fig. 2 shows a chemically etched cross-section of a SPSed compact at 480 °C and extruded composite. The boundary which is coexisting of the CNTs was clearly viewed by the employed etchant (5% sodium hydroxide solution) as shown in Fig. 2a. Thus, the network of etched grooves of uniform thickness implies that all of the CNTs are uniformly arranged in the boundary layer. The particle sizes for all of the matrices produced were almost the same as that of the starting Al particle size, regardless of the high SPS temperature of 480, 500, 560, or 600 °C. This may be due to the fact that grain growth was suppressed by rapid heating (40 °C/min) and the applied pressure during the SPS process, which is termed the "pinning effect". The pinning effect is not affected by the SPS temperature; as shown in Table 1, around 96% density was consistently achieved. We have also confirmed the same result after the extrusion process, an even higher density of about 98% being achieved (Table 1). This implies that the microstructure of the chemically etched extruded composite was extended in parallel in the extrusion direction and the grain size (Al particles) was reduced to around 1 μm along the minor axis as shown in Fig. 2b. The CNTs in the grain boundaries were also oriented in the extrusion direction. Distinct interfacial defects between the CNTs and matrices were hardly observed (the void on the right-hand-side in the inset is mostly an etch groove).

Raman spectroscopic measurements [25] were carried out to assess whether our process (SPS and extrusion) might have affected the local structure of the CNTs due to the high energy consuming processes employed. The I_D/I_G ratios (representing the degree of defects in the CNTs) of SPSed compacts were slightly reduced compared to that of heat-treated Al–CNT powder, as shown in Table 1. It is believed that the residence stress of the CNTs is released during the SPS process as a result of the processing temperature. Also, the I_D/I_G ratios of the extruded composites were a little increased, within an acceptable error range (10%), by high mechanical pressure. Fig. 3 shows the Raman spectra of the extruded composites. These results verified that the SPS and extrusion processes were effective in serving to consolidate the Al–CNT without having any significant effect on the CNTs.

The stress versus strain curves of the extruded Al–CNT composites at various temperatures have been obtained in comparison

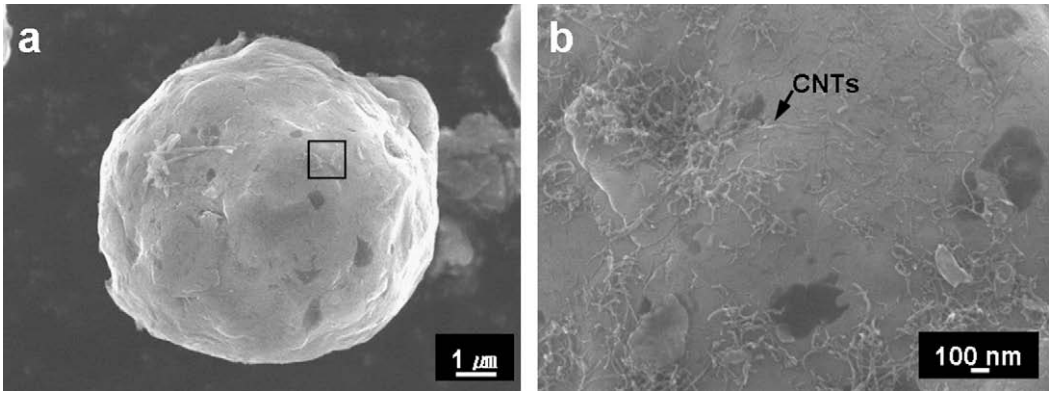

Fig. 1. FE-SEM images of the Al–CNT mixed powder after debinding of natural rubber. (a) Spherical morphology of an Al particle. (b) Higher-magnification image of the surface of an Al–CNT mixed particle (a black arrow indicates a CNT on the Al surface).

Table 1
Relative density and I_D/I_G ratio of SPSed compact and extruded composite depending on SPS temperatures, and mechanical properties of extruded composites (all of the obtained data relate to 1 vol.% CNT addition).

Sample	SPS	Density (g/cm^3)		I_D/I_G (±10%)		Mechanical properties	
	Temperature (°C)	Compact^	Composite^v	SPS	Extrusion	Tensile strength (MPa ± 10%)	Elongation (% ±10%)
Al bulk	600	2.700	2.700	–	–	52	19.5
Heat-treated Al–CNT powder	–	–	–		0.83	–	–
	480	2.469	2.642	0.75	0.82	207.5	21.4
Al–CNT	500	2.575	2.647	0.68	0.81	199.7	20.2
SPSed compact^/composite^v	560	2.607	2.655	0.77	0.77	200.1	19.8
	600	2.593	2.655	0.72	0.79	198.8	18.6

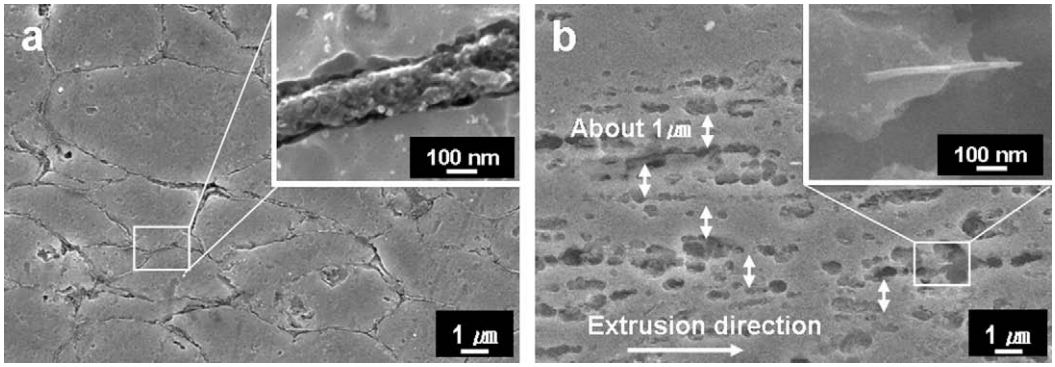

Fig. 2. FE-SEM images of a chemically etched cross-section for the Al/CNT SPSed compact and extruded composite. (a) CNTs are homogeneously distributed in the boundary zone (the inset indicates that the average thickness of the boundary layer is 100 nm). (b) The matrix incorporating CNTs was aligned in the extrusion direction and the minor axis was grown to an average size of 1 μm. The etch pits and grooves were formed selectively around the CNTs (a and b).

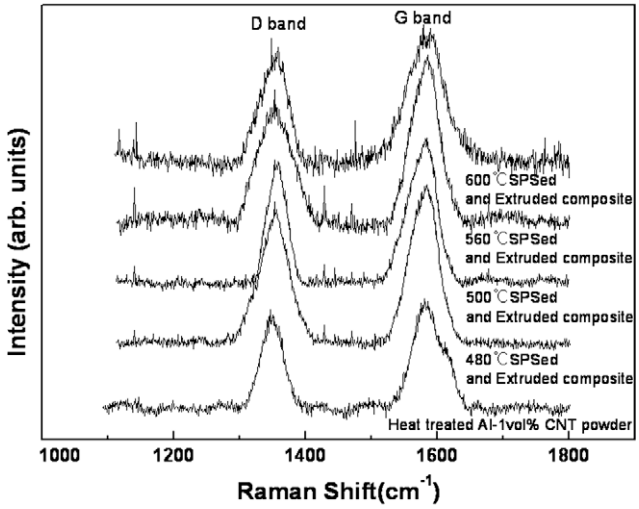

Fig. 3. Raman spectra of SPSed and extruded composites.

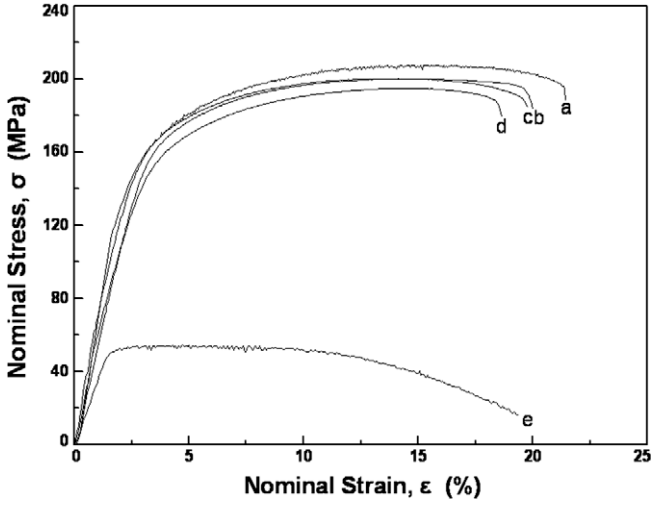

Fig. 4. Nominal stress–strain curves of extruded Al–CNT composites for SPS temperatures of (a) 480, (b) 500, (c) 560, and (d) 600 °C, and (e) extruded pure Al at 600 °C. (a)–(d) show almost the same behavior, having a 300% enhancement compared to (e), extruded pure Al, in spite of the same process being employed.

with that of extruded pure Al, as shown in Fig. 4. The extruded composites exhibited a tensile strength of around 200 MPa, which is 300% higher than that of the extruded pure Al, as indicated Table 1. Pure Al subjected to the same process maintains the same grain size in composites, demonstrating that this remarkable enhancement does not include contributions from work-hardening or grain-refinement effects [18,28,29]. Surprisingly, no decrease in elongation was detected in the Al–CNT composite. The tensile strength and elongation in the Al–CNT composite decreased by around 5.7% and 16%, respectively, on increasing the employed SPS temperature to 480 and 600 °C, demonstrating that control of the SPS temperature may be an important parameter in controlling tensile strength and elongation. George et al. [12] have assessed three different mechanism models (thermal mismatch, Orowan looping, and shear-lag theory) for the strengthening of CNT-reinforced composite materials [14]. However, there is still no clear strengthening mechanism theory for CNT-reinforced metal–matrix composites. Recently, Esawi et al. reported that Al composite reinforced with CNTs (2 wt.%), prepared by their own method, displayed a tensile strength of 345 MPa as compared to 284.5 MPa for pure Al, which represents an enhancement of about 20%. However, their process involved some post-treatment [26]. In the present work, a 300% increase in tensile strength was obtained by adding just 1 vol.% CNTs to Al composite without any post-treatment. Moreover, the stress–strain curves indicate abrupt fractures just before the break, as typically seen for brittle materials (Fig. 4). It is attribute that the obtained microstructure could allow ideal load transfers from the matrices to the CNTs [18,27–30]. Therefore, the abrupt fracture corresponds to the sudden fracture of CNTs by effective load transfer. The obtained Al–CNT composites displayed mainly ductile fracture behavior.

As can be seen in Fig. 5, two different types of aluminum carbide (Al_4C_3) were observed in the boundary zone, dumbbell and tube types. The formation of Al_4C_3 is attributed to chemical reaction between Al and disordered CNTs (=defective CNT) or the tip of a CNT [18,24,31] during the combined processes. We believe that dumbbell-shaped Al_4C_3 originated from the tip of a CNT, whereas tube-shaped Al_4C_3 originated from defective CNTs. It is supposed that the generated Al_4C_3 is not only stabilized on the surface of the tip or defective CNT, but also plays an important role in stress transfer from the Al matrix to the CNTs in Al–CNT composites.

We note that this phenomenon of stress transfer is in accordance with the observed mechanical performance of the Al–CNT composite, especially the fact that there is no degradation of elongation. It is known that Al_4C_3 is easily decomposed in a hygroscopic atmosphere and is characterized by brittleness [32]. So, the obtained Al–CNT composite was aged in water for 24 h, which resulted in our composite being negligibly affected by water. This may be due to the generated Al_4C_3 in the nanosized carbide. In the case of the tube-shaped carbide, which is implanted in the

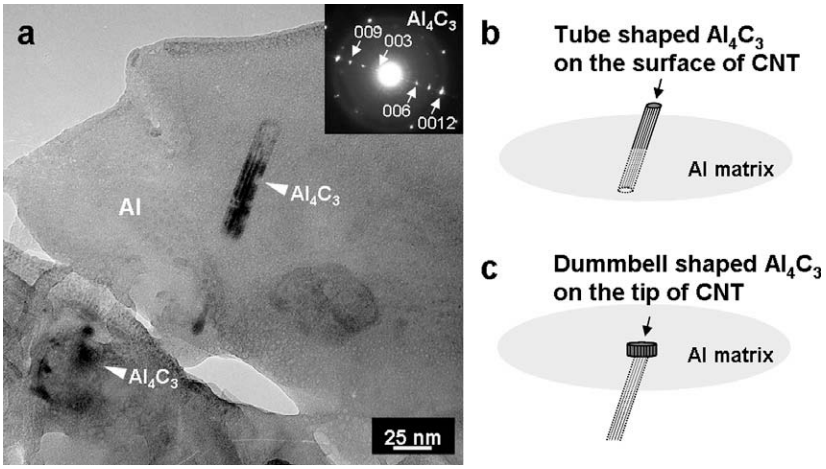

Fig. 5. HR-TEM images of the microstructure of Al–CNT subjected to the extrusion process. (a) The formation of Al_4C_3 was observed near the boundary zone. The inset confirms the crystal structure of Al_4C_3 by its selected-area diffraction (SAD) pattern. (b), (c) Tube-shaped Al_4C_3 was generated on the surface of defective CNTs, whereas particle-shaped Al_4C_3 was generated on the tips of CNTs. Both forms (b) and (c) were implanted into the Al matrix.

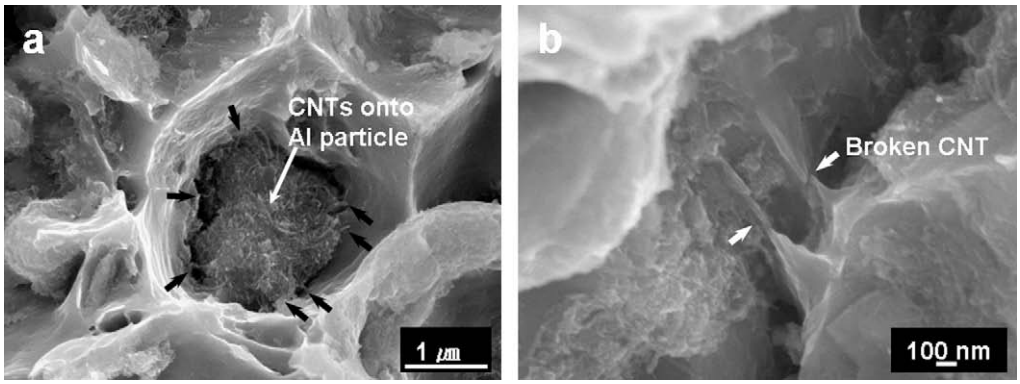

Fig. 6. FE-SEM images of: (a) the fracture surface of the extruded Al–CNT composite after a tensile test, where the black arrows indicate bridging, and (b) higher-magnification image of the inner edge of a dimple bottom, where the white arrows indicate fractured CNTs.

matrix as shown in Fig. 5, the formed carbide may function as a supporting medium to transfer stress from the matrix to the CNTs. Moreover, despite the generation of Al_4C_3, the I_D/I_G ratios of the SPSed compact and extruded composites were lower than that of heat-treated Al–CNT powder. This implies that the I_D/I_G ratio affected the release of residence stress of the CNTs, as is evident from Table 1. This explanation will be investigated in detail in our future work.

The fractographies of the composite after the tensile test are shown in Fig. 6. The fracture surface displayed a lot of dimples associated with ductile fracture, as shown in Fig. 6a. The appearance of dimples means that the interfaces between the Al particles were very strongly metal–metal bonded. The bridgings were obviously formed by CNTs encapsulated in the matrix (see the black arrow in Fig. 6a). Furthermore, no pulled-out CNTs were observed, although some broken CNTs were seen after the tensile tests (see the white arrow in Fig. 6b). The results imply that stress was transferred effectively through the carbides.

The fact that the prepared Al–CNT composite displays highly enhanced tensile strength and elongation with only 1 vol.% CNT addition indicates a resistance to plastic deformation in the stressed state due to difficulty in the rearrangement of dislocations. This phenomenon increases dramatically in micro-ordered structures due to little generated dislocation (meaning limited movement of dislocations) [33]. The CNTs in our composite were selectively distributed around the boundary zone on the nanoscale. This may be one of the reasons why our composite was highly enhanced in terms of tensile strength and elongation. As a result, a remarkable enhancement in tensile strength and no decrease in elongation of the Al–CNT composite could be achieved simultaneously. In addition, the extrusion pressure enhanced the adhesion between the CNTs and matrices.

4. Conclusions

We have achieved enhanced tensile strength with no degradation of elongation in Al–CNT composite containing 1 vol.% CNT due to successful control of the boundary layer. The boundary layers of the composites were around 100 nm on average. In particular, a small quantity of aluminum carbide was generated in the boundary in tube and sand-particle shapes, which may assist effective load transfer from the matrix to the CNTs through chemical bonding. Consequently, it is believed that our approach offers potential for the fabrication of CNT-reinforced Al and Al alloys as a next generation of ultra-light materials with high strength.

Acknowledgements

This research was supported by the New Energy and Industrial Technology Development Organization (NEDO) of Japan. We would also like to acknowledge Nissin Kogyo Co. Ltd. for their technical support.

References

[1] Iijima S. Helical microtubules of graphitic carbon. Nature 1991;354:56–8.
[2] Endo M, Koyama T, Hishiyama Y. Structural improvement of carbon fibers prepared from benzene. Jpn J Appl Phys 1976;15:2073–6.
[3] Esawi A, Farag M. Carbon nanotube reinforced composites: potential and current challenges. Mater Des 2007;28:2394–401.
[4] Ci L, Suhr J, Pushparaj V, Zhang X, Ajayan PM. Continuous carbon nanotube reinforced composites. Nano Lett 2008;8:2762–6.
[5] Sun Y, Sun J, Liu M, Chen Q. Mechanical strength of carbon nanotube–nickel nanocomposites. Nanotechnology 2007;18:505704-1–4-7.
[6] Zhan GD, Kunts JD, Wan J, Mukherjee AK. Single-wall carbon nanotubes as attractive toughening agents in alumina-based nanocomposites. Nat Mater 2003;2:28–38.
[7] Estili M, Kawasaki A. An approach to mass-producing individually alumina-decorated multi-walled carbon nanotubes with optimized and controlled compositions. Scr Mater 2008;58:906–9.
[8] Lau K, Shi S. Failure mechanics of carbon nanotube/epoxy composites pretreated in different temperature environments. Carbon 2002;40:2965–8.
[9] Wong M, Paramsothy M, Xu X, Ren Y, Li S, Liao K. Physical interactions at carbon nanotube–polymer interface. Polymer 2003;44:7757–64.
[10] Coleman J, Khan U, Gunko Y. Mechanical reinforcement of polymers using carbon nanotubes. Adv Mater 2006;18:689–706.
[11] Yea M, Tai N, Liu J. Mechanical behavior of phenolic-based composites reinforced with multi-walled carbon nanotubes. Carbon 2006;44:1–9.
[12] George R, Kashyap KT, Rahul R, Yamadagni S. Strengthening in carbon nanotube/aluminium (CNT/Al) composites. Scr Mater 2005;53:1159–63.
[13] Esawi AMK, Morsi K. Dispersion of carbon nanotubes (CNT) in aluminium powder. Compos Part A: Appl Sci Manuf 2007;38:646–50.
[14] Sridhar I, Narayana KR. Processing and characterizations of MWCNT-reinforced aluminum matrix composites. J Mater Sci 2009;44:1750–6.
[15] Deng C, Zhang X, Ma Y, Wang D. Fabrication of aluminum matrix composite reinforced with carbon nanotubes. Rare Metals 2007;26:450–5.
[16] Esawi A, Borady M. Carbon nanotube-reinforced aluminium strips. Compos Sci Technol 2008;68:486–92.
[17] Kuzumaki T, Miyazawa K, Ichinose H, Ito K. Processing of carbon nanotube reinforced aluminum composite. J Mater Res 1998;9:2445–9.
[18] Kwon H, Estili M, Takagi K, Miyazaki T, Kawasaki A. Combination of hot extrusion and spark plasma sintering for producing carbon nanotube reinforced aluminum matrix composites. Carbon 2009;47:570–7.
[19] Omori M. Sintering, consolidation, reaction and crystal growth by the spark plasma system (SPS). Mater Sci Eng A 2000;287:183–8.
[20] Xie G, Ohashi O, Yoshioka T, Song M, Mitsuishi K, Yasuda H, et al. Effect of interface behavior between particles on properties of pure Al powder compacts by spark plasma sintering. Mater Trans 2001;42:1846–9.
[21] Galanty M, Kazanouski P, Kansuwan P, Misiolek W. Consolidation of metal powders during the extrusion process. J Mater Process Technol 2002;125:491–6.
[22] Yuuki J, Kwon H, Kawasaki A, Magario A, Noguchi A, Beppu J, et al. Fabrication of carbon nanotube reinforced aluminum composites by powder extrusion process. Mater Sci Forum 2007;53:889–92.
[23] Noguchi T, Magario A, Fukazawa S, Shimizu S, Beppu J, Seki M. Carbon nanotube/aluminium composites with uniform dispersion. Mater Trans 2004;45:602–4.
[24] Kwon H, Kawasaki A. Extrusion of spark plasma sintered aluminum–carbon nanotube composites at various sintering temperatures. J Nanosci Nanotechnol 2009;9:6542–8.
[25] Zhao Q, Wagner HD. Raman spectroscopy of carbon-nanotube-based composites. Philos Trans Roy Soc A 2004;362:2407–24.
[26] Esawi AMK, Morsi K, Sayed A, Gawad AA, Borah P. Fabrication and properties of dispersed carbon nanotube–aluminum composites. Mater Sci Eng A 2009;508:167–73.
[27] Fukuda H, Chou TW. A probabilistic theory of the strength of short-fibre composites with variable fibre length and orientation. J Mater Sci 1982;17:1003–11.
[28] Kelly A, Tyson WR. Tensile properties of fibre-reinforced metals: copper/tungsten and copper/molybdenum. J Mech Phys Solids 1965;13:329–38.
[29] Cox HL. The elasticity and strength of paper and other fibrous materials. Brit J Appl Phys 1952;3:72–9.
[30] Lourie O, Wagner HD. Evidence of stress transfer and formation of fracture clusters in carbon nanotube-based composites. Compos Sci Technol 1999;59:975–7.
[31] Ci L, Ryu Z, Jin-Phillipp NY, Rühle M. Investigation of the interfacial reaction between multi-walled carbon nanotubes and aluminum. Acta Mater 2006;54:5367–75.
[32] Khalid FA, Beffort O, Klotz UE, Keller BA, Gasser P. Microstructure and interfacial characteristics of aluminum–diamond composite materials. Diam Relat Mater 2004;13:393–400.
[33] Oh SH, Legros M, Kiener D, Dehm D. In situ observation of dislocation nucleation and escape in a submicrometre aluminium single crystal. Nat Mater 2009;8:95–100.